

## Water Splitting | Very Important Paper |

VIP Substituent-Induced Deformed Ni–Porphyrin as an  
Electrocatalyst for the Electrochemical Conversion of Water into  
Dioxygen

Jonnadula Venkata Suman Krishna,<sup>[a,b]</sup> Narra Vamsi Krishna,<sup>[a,b]</sup> Santosh K. Singh,<sup>[b,c]</sup>  
Pankaj K. Shaw,<sup>[d]</sup> Vishal M. Dhavale,<sup>\*[a]</sup> Anil Kumar Vardhaman,<sup>\*[a]</sup> and  
Lingamallu Giribabu<sup>\*[a,b]</sup>

**Abstract:** The electrochemical water oxidation ability of complexes 5,15-diphenylporphinatonickel(II) (**A**) and 5,15-bis(3,5-di-*tert*-butylphenyl)porphinatonickel(II) (**B**) in the oxygen evolution reaction (OER) have been investigated in an alkaline medium. Complex **B** was found to be kinetically and thermodynamically more active than complex **A**. The overpotential and Tafel slope of complex **B** are lower than those of complex **A** by 30 mV and around 45 mV/decade, respectively, which supports the higher activity of **B**. Moreover, stability tests endorse the sustainability of both samples under alkaline conditions. It has

been found that the 3,5-di-*tert*-butylphenyl substituent in **B** plays a decisive role in achieving a better OER onset potential and current than that obtained with **A**, which is a result of the modulation of the structural parameters of **B**. Furthermore, the measured OER activities of **A** and **B** have been correlated with their molecular arrangement as well as differences in their bonding characteristics and dipole moments. For further insight, the obtained results have been confirmed by a theoretical study.

## Introduction

With a view to renewable energy, the oxidation of water is an important reaction for generating fuel and oxidants, depending on the catalyst used and the operational conditions.<sup>[1]</sup> The oxidation of water to produce oxygen involves four protons and four electrons, which indicates a complex reaction with respect to thermodynamics and kinetics.<sup>[1]</sup> Hence, the development of a catalyst to mimic water oxidation (WO) in natural photosynthesis, which can operate at a lower overpotential, is of paramount importance to the scientific community.<sup>[1]</sup> To date, iridium and ruthenium oxides have been considered as standard electrocatalysts for WO, but cost is a major stumbling block for their widespread use.<sup>[2–4]</sup> Moreover, metals, metal oxides, and metal hydroxides in supported and/or nonsupported systems

are currently used as heterogeneous electrocatalysts and they show promising activity in electrochemical WO (EcWO) in comparison with homogeneous metal complex systems.<sup>[1,5–11]</sup> Despite this, heterogeneous electrocatalysts are lagging behind homogeneous systems due to the difficulty in predicting the mechanisms of their action, the poor reproducibility of electrocatalysts with the same number of active sites, and limitations of structural modulation, which block their further development and application in EcWO.<sup>[5b,7a]</sup> In contrast, homogeneous electrocatalysts such as molecular complexes have potential to solve all the problems mentioned above, owing to the possibility of predicting the mechanistic pathways as well as the high reproducibility of the complexes and results,<sup>[1b,5a,7b–7d]</sup> even though during the EcWO process the homogeneous electrocatalyst may undergo decomposition and/or transform into a heterogeneous substrate that still acts as an active electrocatalyst.<sup>[12,13]</sup> Under these circumstances, gaining a better understanding of the system is complicated. However, mono-metal-ion-centered systems always allow for the optimization of the activity, selectivity, and stability of heterogeneous electrocatalysts.<sup>[14]</sup> In view of this, the use of metal–organic networks, covalent organic frameworks, and metal complexes in the WO reaction have been investigated by researchers, but they have failed to predict the exact active catalytic center and the mechanism.<sup>[8,15–18]</sup> This could be due to the decomposition/transformation of the catalyst under the operating conditions.<sup>[12,13,20]</sup> In addition to this, their low conductivity is a further issue. To overcome this problem, researchers have prepared composites and/or mixed the catalysts with conducting carbon and observed improvements in current during the WO process.<sup>[15,19]</sup>

[a] *Inorganic and Physical Chemistry Division, CSIR-Indian Institute of Chemical Technology, Uppal Road, Tarnaka, Hyderabad 500 007, India*  
E-mail: vishal.mdhavale@gmail.com  
anil1hnk@gmail.com  
giribabu@iict.res.in  
<http://www.iictindia.org>

[b] *Academy of Scientific and Innovative Research (AcSIR), Anusandhan Bhawan, 2 Rafi Marg, New Delhi, 110001, India*

[c] *Physical and Materials Chemistry Division, CSIR-National Chemical Laboratory, Pune, 411 008, India*

[d] *Centre for Material Characterisation, CSIR-National Chemical Laboratory, Pune, 411 008, India*

 Supporting information and ORCID(s) from the author(s) for this article are available on the WWW under <https://doi.org/10.1002/ejic.201701427>.

Under these conditions, the interaction between the carbon and single-atom system makes it more difficult to understand the reaction pathways. Hence, the current need is to have a complex electrocatalyst with a single active site that shows oxygen evolution reaction (OER) activity with reasonable current output and makes the system more understandable. The electrocatalytic activities of metal complexes can be tuned by modifying the ligand and their nature (i.e., electron-donating/withdrawing). The electronic effect induced by ligand substituents plays a vital role in redefining the redox properties of metal complexes.<sup>[21]</sup> Besides this, to date, structural changes in mono-metal-ion-centered complex electrocatalysts are not fully understood by researchers, because their structures and properties are greatly influenced by the substituents or ligands, and, to the best of our knowledge, so far, no one has tried to explore these effects. However, by gaining an understanding of these effects, it will be very easy to tune the properties and engineer the desired single-site electrocatalysts, that is, molecular electrocatalysts. With this in mind, in this work we have prepared Ni-porphyrin complexes with phenyl and 3,5-di-*tert*-butylphenyl substituents as heterogeneous (water insoluble) electrocatalysts for the OER in an alkaline medium and they were found to be chemically more stable under these conditions. The better ability of the Ni center to adsorb oxygen species and, importantly, the fact that it is a single-site electrocatalyst, allows the OER pathway to be predicted.<sup>[22,23]</sup> Hence, researchers are focusing their interest on Ni-based systems. Moreover, the effect of induced structural deformation and the change in the dipole moments of the Ni-porphyrin system by variation of the substitution has also been studied and the results have been confirmed by a theoretical optimization study.

## Results and Discussion

Initially, the structures of **A** and **B** were confirmed by <sup>1</sup>H NMR and MALDI-TOF mass spectral analyses. The <sup>1</sup>H NMR spectra of **A** and **B** are shown in Figures S2 and S4 in the Supporting Information and the MALDI-TOF mass spectra in Figures S3 and S5, respectively, and the corresponding data are provided in the Exptl. Sect. The morphologies of **A** and **B** were determined by scanning (SEM) and transmission electron microscopy (TEM) and are displayed in Figure 1. It can be seen from the SEM image that **A** stacks as sheets and self-arranges to form block-type structures (Figure 1a), whereas the TEM images reveal sheet structures (Figure 1a',a''). The differences in the SEM and TEM images could be due to the difference in sample preparation methods adopted. We believe that the observed morphology is due to the planar nature of **A**, which allows molecules to stack together through  $\pi$ - $\pi$  interactions. On the other hand, **B** has a spherical flake-type morphology (Figure 1b-b''). It can be predicted from the images that in both cases the cooperative square-planar geometries of the Ni-porphyrin complexes and the synergetic interactions between them play a decisive role in achieving the said structures.

The UV spectra of **A** and **B** and their respective non-metal complexes are shown in Figure S6 in the Supporting Information. Comparison of the spectra reveal a reduction in the num-

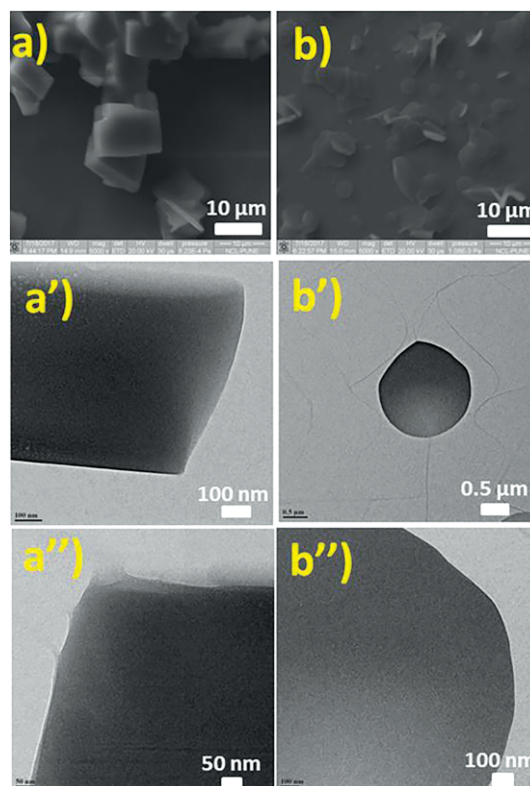


Figure 1. Morphologies of **A** and **B**. SEM (a and b) and TEM (a',a'' and b',b'') images for **A** and **B**, respectively, at different magnifications.

ber of Q-bands after the insertion of the metal ion into the ligand, which confirms the successful formation of the Ni-porphyrin complexes.<sup>[27,28]</sup> In addition, the observed shift in the Q-band upon complex formation can be attributed to the interaction between the Ni metal ion and the N atoms of the porphyrin ligands.

Furthermore, from a theoretical study performed with the Gaussian 09 software, detailed structural features of **A** and **B** were identified. Frontier molecular orbital (FMOs) reveal the position of the electron density (see Figures S7 and S8 in the Supporting Information), and their geometries were found to be stable in their projected conformations (Figure 2). The energy of **B** was calculated to be nearly 1.2 times higher than that of **A** (see Table S1), and the dipole moment of **B** (0.5545 Debye) is also greater than that of **A** (0.0003 Debye; Table S1). Overall, the differences in the energy, dipole moment, and angle between the porphyrin and phenyl substituent contribute to the deformation observed in molecule **B** (Figure 2) and the disparity of the charge distribution in the same (see Figures S7 and S8). Additionally, all four Ni-N bond lengths were found to be the same in **A** (1.957 Å) and, as a result, the optimized structure has a planar geometry (see Figure S1a' and Figure 2a-2a''), whereas **B** has similar Ni-N bond lengths (ca. 1.93 Å, see Table S1), but are shorter than those observed in **A**, revealing the influence of the *tert*-butyl substituent, which results in the deformation of the molecule (Figure 2) with a higher dipole moment, as discussed above. All the above-mentioned parameters are presented in Table S1.

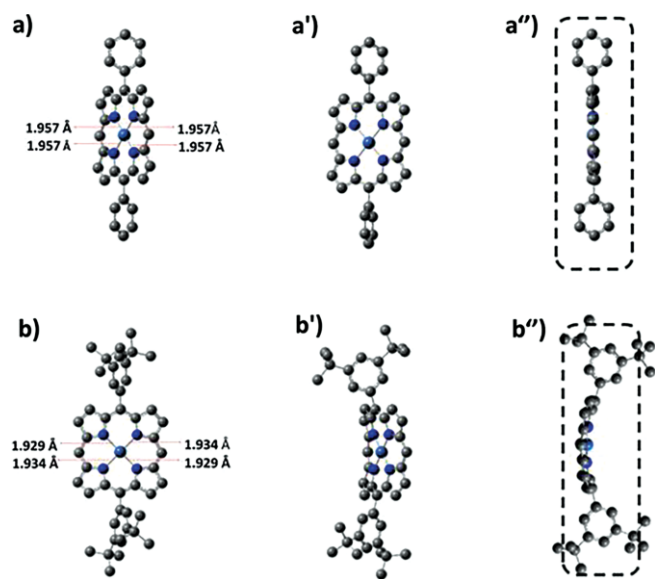


Figure 2. Theoretically optimized structures of (a–a'') **A** and (b–b'') **B** viewed from different angles to show the deformation of the structures and the bending/curving of the porphyrin rings due to the substituents. All the structures are shown without hydrogen atoms for the purpose of clarity.

On the basis of the above-discussed physicochemical and structural data for **A** and **B**, we investigated their potential application in the EcWO. We studied their EcWO activity in an

alkaline medium and found that **B** is better than **A** under these conditions. Initially, cyclic voltammograms (CVs) were recorded in a 0.1 M aq. KOH solution at different scan rates and are presented in Figures S9a and S10a in the Supporting Information. Ni<sup>2+/3+</sup> redox behavior was observed in the potential range of 1.3–1.6 V versus RHE. The slight deviation in the peak potentials of **A** and **B** has been attributed to the different substituents in the Ni–porphyrin complexes (see Figure S11). The observed increase in current with respect to the square root of the scan rate indicates the diffusion-controlled nature of the peaks<sup>[15,19]</sup> of the Ni redox couple (see Figures S9b and S10b). Furthermore, the EcWO ability was tested by linear sweep voltammetry (LSV) in an alkaline medium and the voltammograms are shown in Figure 3a.

The sharp increment in current after the oxidation peak was due to the conversion of water into dioxygen. The onset potentials of the EcWO leading to oxygen evolution were found to be 1.63 and 1.60 V versus RHE for **A** and **B**, respectively (Figure 3b). Furthermore, the overpotential values for **A** and **B** were calculated from the onset potentials and found to be 0.40 and 0.37 V, respectively (Figure 3b). Tafel slopes were obtained by plotting  $\log j$  versus the potential (Figure 3c).<sup>[29]</sup> The lower Tafel slope of **B** (122.76 mV/decade) in comparison with that of **A** (167.72 mV/decade) indicates that **B** is more likely to undergo the OER than **A**. Besides this, the lower Tafel slope of **B** provides information on the viability of the OER mechanism, which is influenced by

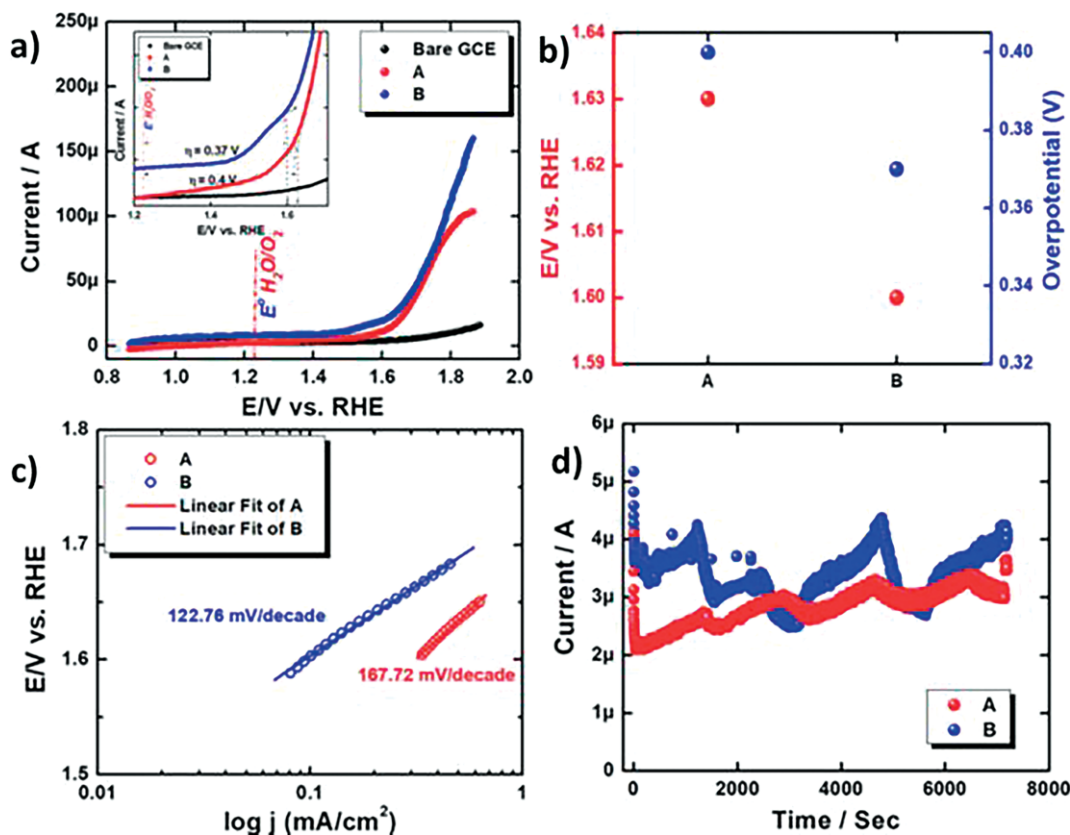


Figure 3. (a) Linear sweep voltammograms (LSVs) for **A**, **B**, and a bare glassy carbon electrode (GCE) recorded at a scan rate of 20 mV/s. (b) Onset potentials and overpotentials for **A** and **B**. (c) Tafel plots of **A** and **B**. (d) Stability tests for **A** and **B** (in this case, the current vs. time test was conducted at a constant applied potential of 1.7 V vs. RHE for 7200 s).

the nature of the adsorption of oxygen species and the variation in their coverage with respect to the potential. This was found to be more effective for **B** than for **A** (Figure 3a,b). Furthermore, the current obtained was also found to be higher for **B** than for **A**. These results indicate that **B** is thermodynamically and kinetically more active than **A**. Overall, the differences in the results can be attributed to the difference in their dipole moment (due to a variation in the charge distribution) and the deformation of molecule **B** (i.e., the difference in the angle between the porphyrin and phenyl groups, which results in the bending/curving of the porphyrin), which is induced by the substituent on the Ni-porphyrin and is also affected by the Ni-N bonding characteristics (see Table S1), leading to an increase in the strain in the molecule.

Because **A** and **B** both possess a Ni center, which is considered to be the active site for the EcWO leading to oxygen evolution, we believe that the EcWO with **A** and **B** might follow the same mechanistic pathway, as reported by Han and Usov et al.<sup>[22,23]</sup> and presented in Figure 4. In detail, initial loss of an electron (oxidation of the Ni-porphyrin) generates the radical cation (Figure 4,I). Subsequently, a molecule of water interacts with the Ni center of the porphyrin (Figure 4,II). The bonded water molecule deprotonates with the simultaneous loss of an electron resulting in a hydroxide-bonded Ni-porphyrin system (Figure 4,III). Next, rupture of the O-H bond and subsequent intramolecular transfer of an electron to the porphyrin core

coupled with proton loss results in the formation of a Ni-porphyrin oxo radical (Figure 4,IV).

In the next step, internal proton transfer leads to the formation of Ni-porphyrin hydroperoxide (Figure 4,V), which forms the superoxide radical of Ni-porphyrin (Figure 4,VI) with the loss of a proton and electron. Then a final oxidation step leads to the release of oxygen and regenerates the initial Ni-porphyrin complex. Overall, from the probable mechanistic pathway, we can conclude that the active center plays a major role and determines the reaction path towards the desired product. In addition to this, the influence of the molecular structure on the overall activity also plays a major role in the design of OER active catalysts. Moreover, the stabilities of **A** and **B** were confirmed by measuring the current output with respect to time at a constantly applied overpotential of 0.47 V, which is slightly higher than the actual overpotential (which was calculated from the onset potential), and the data are shown in Figure 3d. The current obtained with **B** is slightly higher than that obtained with **A**. Both samples show some fluctuations during the measurement. This behavior could be due to the formation of oxygen bubbles on the surface of the working electrode, which we removed by in situ nitrogen purging.

An electrochemical analysis of the ligands (**LA** and **LB** ligands of **A** and **B**, respectively) was undertaken in a 0.1 M KOH solution. Figures S12 and S13 in the Supporting Information show the CVs of **LA** and **LB** recorded at different scan rates (details are given in the Supporting Information) and the LSVs of **LA** and **LB** are displayed in Figures S14 and S15. The CVs and LSVs of the ligands show very low current output without any characteristic features, whereas the Ni-inserted porphyrins, that is, **A** and **B**, show characteristic features and electrocatalytic ability. The LSVs of **A** and **B** before and after the stability test are shown in Figure 5. The onset potentials of the OER are observed to be at around 1.63 and 1.6 V versus RHE for **A** and **B**, respectively. Before the stability test, **A** and **B** show currents of around 100 and 160  $\mu\text{A}$ , respectively, at 1.9 V versus RHE, which increases to around 210 and 350  $\mu\text{A}$ , respectively, after the stability test. This improvement in current can be attributed to the improved accessibility of the ions and increased exposure of the active sites due to prolonged application of potential. It can also be attributed to the improved hydrophilic characteristics of the electrocatalysts under the application of potential. These are a few possible reasons for the improvement in the current (Figure 5). Other factors may also be responsible for this improvement and we are working towards their confirmation. The constant onset potential value for both samples before and after the stability test indicates better sustainability of the samples in alkaline solution and under the operating conditions. Gas chromatography was used to confirm the evolution of oxygen (see Figures S22 and S23). The area under the chromatograph was found to be slightly higher for **B** than for **A**, and hence we believe that **B** has greater potential in the OER than **A**. Furthermore, to confirm that the molecular complex and nickel remain intact, we performed a MALDI-TOF mass spectral measurement on the samples collected after the stability test and found them to be the same (see Figures S16 and S17) as those observed before the test. In addition, we per-

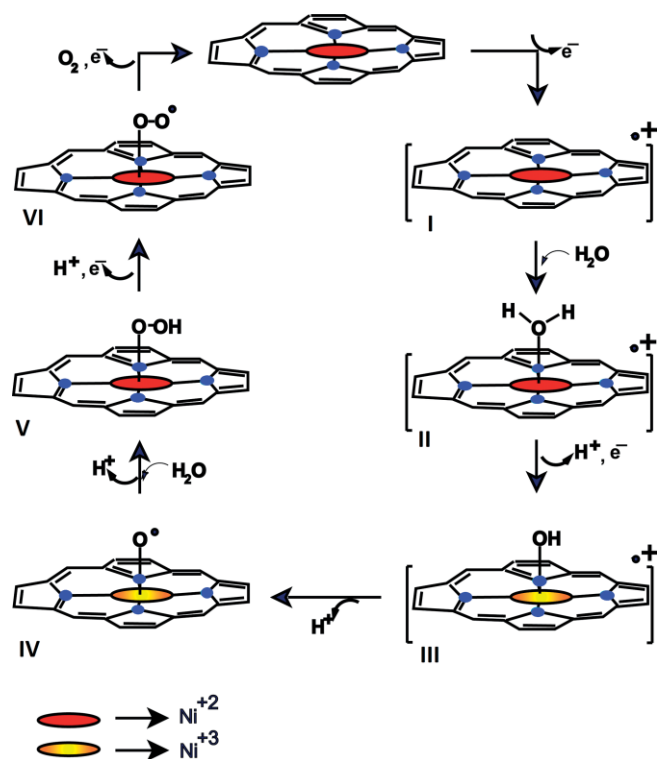


Figure 4. Hypothetical mechanistic pathway for the EcWO leading to oxygen evolution for a general porphyrin system.<sup>[22,23]</sup> Here, for a better understanding and greater clarity, we have omitted the substituents and the mechanism is proposed to involve only the Ni-porphyrin core. The blue dots represent the porphyrin nitrogen atoms, which are bonded to the nickel centre.

formed a UV/Vis measurement on the samples collected after the OER study (see Figures S18 and S19) and just after the starting of the OER (see Figures S20 and S21) and found them to be the same as those observed before the test. The better activity caused by the *tert*-butyl groups in complex **B** could be due to the combined effects of structural deformation, bonding characteristics, and electronic effect, which is induced by the substituent, but we believe that the change in the dipole moment, angle between the porphyrin and phenyl group, and Ni–N bond lengths (Table S1) play a decisive role. All these differences work in the favor of **B**. However, to draw some conclusions as to the electronic effect, a more detailed analysis is needed, which is underway in our laboratory. Also, the structural stability of **B** can be attributed to the geometry of the molecule, the molecular deformation, and the shorter Ni–N bond lengths etc. Overall, the properties of **B** have been shown to be important for the EcWO. In addition, the bending/curving of the Ni–porphyrin structure in the presence of the *tert*-butyl substituents helps **B** to excel. Hence, judicious selection of substituents can change the entire nature of porphyrins to allow them to be applied in the field of electrochemical power sources. Our study may help researchers to design an efficient molecular electrocatalyst for the generation of oxygen and hydrogen from water and for the effective conversion of CO<sub>2</sub> into value-added compounds.

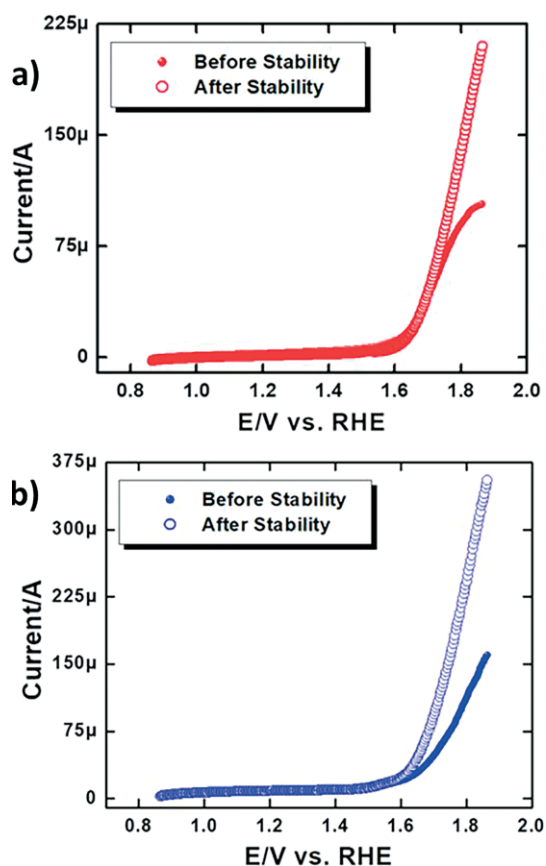


Figure 5. LSVs of a) **A** and b) **B** recorded before and after the stability test. Scan rate, 0.02 V/s; electrolyte, aq. 0.1 M KOH.

## Conclusions

We have reported herein on 5,15-diphenylporphinatonickel(II) (**A**) and 5,15-bis(3,5-di-*tert*-butylphenyl)porphinatonickel(II) (**B**) complexes as chemically stable heterogeneous electrocatalysts for electrochemical water oxidation in the OER in an alkaline medium. The differences in the molecular structure, metal–nitrogen bond lengths, and dipole moment of **B** compared with **A**, resulting from a modification of the substituents, have been found to play a decisive role in achieving better EcWO activity in the OER. Thus, structural modulation/engineering of a molecular complex by the judicious selection of substituents can induce favorable modifications in the structure that might help to create better mono-metal-ion-centered EcWO electrocatalysts for the efficient generation of oxygen from water. In addition, our approach should help the researcher to design further single- and/or multi-metal-ion-centered EcWO electrocatalysts in the future.

## Experimental Section

**Materials:** Pyrrole, benzaldehyde (**1**), 3,5-di-*tert*-butylbenzaldehyde (**2**), paraformaldehyde (HCHO), trifluoroacetic acid (TFA), sodium hydroxide, potassium hydroxide, *n*-butyllithium, 2,3-dichloro-5,6-dicyano-1,4-benzoquinone (DDQ), and 1-bromooctane were purchased from Sigma–Aldrich. Dimethylformamide (DMF), tetrahydrofuran (THF), tetramethylethylenediamine (TMEDA), potassium carbonate, dichloromethane (DCM), and nickel(II) acetate [Ni(OOCCH<sub>3</sub>)<sub>2</sub>·4H<sub>2</sub>O] were purchased from Merck and Rankem. Deionized (DI) water was obtained from a Millipore instrument.

**5,15-Diphenylporphinatonickel(II) (A):** In a 100 mL round-bottomed flask a suspension of 5,15-diphenylporphyrin (**5**; 200 mg, 0.432 mmol) and Ni(OOCCH<sub>3</sub>)<sub>2</sub>·4H<sub>2</sub>O (214.9 mg, 0.864 mmol) in DMF (50 mL) was stirred at reflux temperature for 4 h. The reaction was quenched with water (100 mL) and the mixture was extracted with DCM (2 × 100 mL). The combined extracts were washed with water and dried with anhydrous MgSO<sub>4</sub>. The solvent was then removed under reduced pressure and the residue purified by column chromatography using silica gel (80 % DCM/hexane) to afford **A** (185 mg, 85 % yield). <sup>1</sup>H NMR (400 MHz, CDCl<sub>3</sub>): δ = 9.94 (s, 2 H), 9.19 (d, *J* = 4.8 Hz, 4 H), 8.94 (d, *J* = 4.8 Hz, 4 H), 8.07 (dd, *J* = 8.0 Hz, 4 H), 7.72 (m, 6 H) ppm. MS (MALDI-TOF): calcd. for C<sub>32</sub>H<sub>20</sub>N<sub>4</sub>Ni 518.10 [M]<sup>+</sup>; found 518.08. Scheme S1 in the Supporting Information shows the synthetic procedure adopted for the synthesis of **A**. The chemical and theoretical optimized structures of **A** are displayed in Figure S1.

**5,15-Bis(3,5-di-*tert*-butylphenyl)porphinatonickel(II) (B):** In a 100 mL round-bottomed flask a suspension of 5,15-bis(3,5-di-*tert*-butylphenyl)porphyrin (**6**; 200 mg, 0.291 mmol) and Ni(OOCCH<sub>3</sub>)<sub>2</sub>·4H<sub>2</sub>O (144.82 mg, 0.582 mmol) in DMF (50 mL) was stirred at reflux temperature for 4 h. The reaction was quenched with water (100 mL) and the mixture was extracted with DCM (2 × 100 mL). The combined extracts were washed with water and dried with anhydrous MgSO<sub>4</sub>. The solvent was then removed under reduced pressure and the residue was purified by column chromatography using silica gel (90 % DCM/hexane) to afford **B** (180 mg, 80 % yield). <sup>1</sup>H NMR (400 MHz, CDCl<sub>3</sub>): δ = 9.94 (s, 2 H), 9.19 (d, *J* = 4.8 Hz, 4 H), 8.99 (d, *J* = 4.8 Hz, 4 H), 7.94 (d, *J* = 8.0 Hz, 4 H), 7.77 (t, *J* = 8.0 Hz, 2 H), 1.66–1.53 (s, 12 H), 1.52–1.50 (m, 24 H) ppm. MS (MALDI-TOF): calcd. for C<sub>48</sub>H<sub>52</sub>N<sub>4</sub>Ni 742.35 [M]<sup>+</sup>; found 742.31. Scheme S1 in the Supporting Information shows the synthetic pro-

cedure adopted for the synthesis of **B**. The chemical and theoretical optimized structures of **B** are displayed in Figure S1.

**Characterization:** The imaging of both the samples was performed by SEM and TEM. Well-dispersed solutions of **A** and **B** in THF were drop-coated onto a silicon wafer, dried at room temperature, and later used for the SEM imaging, by using Quanta-TM and Nova Nano SEM 450 scanning electron microscopes. In similar way, well-dispersed solutions of **A** and **B** in THF were drop-coated onto a carbon-coated Cu grid (Global Nanotech.), dried at room temperature, and later placed into the chamber to record TEM images with a Tecnai-T 30 high-resolution transmission electron microscope at an accelerated voltage of 200 kV. <sup>1</sup>H NMR spectra of all the prepared samples were recorded with an INOVA spectrometer (frequency: 400 MHz, internal reference: CDCl<sub>3</sub>). Matrix-assisted laser desorption ionization time-of-flight (MALDI-TOF) mass spectrometry was performed with a Shimadzu Biotech Axima Performance spectrometer (2.9.3.20110624: Linear mode, Mode Reflectron\_HiRes). UV/Vis absorption spectra were recorded with a Shimadzu spectrophotometer (Model UV-3600).

**Electrochemical Studies:** All the electrochemical studies were carried out with a CH instrument (Model CH-620E). Cyclic voltammetry, linear sweep voltammetry, and the stability tests were performed by using a three-electrode electrochemical cell in a 0.1 M KOH solution. A glassy carbon electrode (GCE) modified with **A** or **B** was used as the working electrode and Hg/HgO and Pt wires were used as reference and counter electrodes, respectively. The modified GCE was prepared by drop-coating the catalyst slurry prepared with a sample of **A** or **B** in THF solvent. For this, A or B (2.5 mg) was added to THF (1 mL) and sonicated to achieve a well-dispersed mixture. Later, the above mixture (10 μL) was drop-coated onto the GCE surface. In addition to this, a 0.01 % aq. Nafion solution (2.5 μL) was used as binder. Prior to the preparation of the modified GCE electrode, the GCE was mirror-polished with alumina powder and thoroughly washed with copious amounts of DI water. Finally, the electrode was dried in an oven at 60 °C for 2 h. The geometrical area of the GCE was 0.07065 cm<sup>2</sup>. All the electrochemical experiments were performed at room temperature. The CVs were recorded at different scan rates in a potential window of 0.5 to 1.7 V versus RHE. The LSVs were recorded from 0.9 to 1.9 V versus RHE. The stability tests were performed at an applied potential of 1.7 V, that is, an overpotential of 0.47 V for 2 h. All the electrochemical measurements were performed in nitrogen-saturated 0.1 M KOH solution, and all the potentials were converted into the RHE scale by using Equation (1).

$$E_{\text{RHE}} = E_{\text{Hg/HgO}} + 0.098 + 0.0591\text{pH} \quad (1)$$

**Theoretical Study:** The Gaussian 09 software package was employed for the calculations using the B3LYP method and the 6-31G(d,p) basis set. The ground state properties, such as energy-minimized structures and frontier molecular orbitals, were calculated by using DFT in the gas phase.<sup>[24–26]</sup>

**Gas Chromatography Study:** Gas chromatographic analysis was performed with a Varian gas chromatograph (Model: cp3800) equipped with a TCD detector using a Carboxen1000 column. Helium was used as the carrier gas. Before the start of experiments, the electrolyte was purged with nitrogen for 20 min. For the oxygen evolution study we used an overpotential of around 0.47 V and gas chromatographs were recorded in situ. A small pipe was placed in the headspace of the home-made cell and directly connected to the GC instrument for the in situ measurement of the evolved gas.

## Acknowledgments

We would like to acknowledge the CSIR-Indian Institute of Chemical Technology (IICT), Hyderabad for their support. V. M. D., A. K. V., and L. G. acknowledge the DST-Inspire Program (DST/INSPIRE/04/2016/000409), SERB-NPDF (PDF/2016/001158), and DST-SERI, respectively, for financial support. J. V. S. K. thanks the University Grants Commission (UGC), and N. V. K. and S. K. S. acknowledge the Council of Scientific and Industrial Research (CSIR) for research fellowships. We are grateful to Dr. N. Lingaiah, IICT, Hyderabad for the GC measurements.

**Keywords:** Oxygen · Nickel · Porphyrinoids · Electrochemistry · Water chemistry · Electrocatalysts

- [1] a) B. M. Hunter, H. B. Gray, A. M. Müller, *Chem. Rev.* **2016**, *116*, 14120–14136; b) W. Zhang, W. Lai, R. Cao, *Chem. Rev.* **2017**, *117*, 3717–3797.
- [2] A. Harriman, I. J. Pickering, J. M. Thomas, P. A. Christensen, *J. Chem. Soc., Faraday Trans. 1* **1988**, *84*, 2795–2806.
- [3] X. Chen, G. Chen, P. L. Yue, *J. Phys. Chem. B* **2001**, *105*, 4623–4628.
- [4] J. D. Blakemore, N. D. Schley, G. W. Olack, C. D. Incarvito, G. W. Brudvig, R. H. Crabtree, *Chem. Sci.* **2011**, *2*, 94–98.
- [5] a) H. Lei, A. Han, F. Li, M. Zhang, Y. Han, P. Du, W. Lai, R. Cao, *Phys. Chem. Chem. Phys.* **2014**, *16*, 1883–1893; b) C. C. L. McCrory, S. Jung, J. C. Peters, T. F. Jaramillo, *J. Am. Chem. Soc.* **2013**, *135*, 16977–16987.
- [6] J. B. Gerken, J. Y. C. Chen, R. C. Masse, A. B. Powell, S. S. Stahl, *Angew. Chem. Int. Ed.* **2012**, *51*, 6676–6680; *Angew. Chem.* **2012**, *124*, 6780.
- [7] a) R. D. L. Smith, M. S. Prevot, R. D. Fagan, S. Trudel, C. P. Berlinguette, *J. Am. Chem. Soc.* **2013**, *135*, 11580–11586; b) H. Lei, C. Liu, Z. Wang, Z. Zhang, M. Zhang, X. Chang, W. Zhang, R. Cao, *ACS Catal.* **2016**, *6*, 6429–6437; c) L. Xu, H. Lei, Z. Zhang, Z. Yao, J. Li, Z. Yua, R. Cao, *Phys. Chem. Chem. Phys.* **2017**, *19*, 9755–9761; d) H. Sun, Y. Han, H. Lei, M. Chena, R. Cao, *Chem. Commun.* **2017**, *53*, 6195–6198.
- [8] D. Mullangi, V. Dhavale, S. Shalini, S. Nandi, S. Collins, T. Woo, S. Kurungot, R. Vaidhyathanan, *Adv. Energy Mater.* **2016**, *6*, 1600110.
- [9] V. M. Dhavale, S. S. Gaikwad, L. George, R. N. Devi, S. Kurungot, *Nanoscale* **2014**, *6*, 13179–13187.
- [10] N. Ayasha, V. M. Dhavale, S. Kurungot, *Nanoscale* **2017**, *9*, 12590–12600.
- [11] S. K. Singh, V. M. Dhavale, S. Kurungot, *ACS Appl. Mater. Interfaces* **2015**, *7*, 442–451.
- [12] Q. Yin, J. M. Tan, C. Besson, Y. V. Geletii, D. G. Musaev, A. E. Kuznetsov, Z. Luo, K. I. Hardcastle, C. L. Hill, *Science* **2010**, *328*, 342–345.
- [13] Z. Huang, Z. Luo, Y. V. Geletii, J. W. Vickers, Q. Yin, D. Wu, Y. Hou, Y. Ding, J. Song, D. G. Musaev, C. L. Hill, T. J. Lian, *J. Am. Chem. Soc.* **2011**, *133*, 2068–2071.
- [14] X. F. Yang, A. Wang, B. Qiao, J. Li, J. Liu, T. Zhang, *Acc. Chem. Res.* **2013**, *46*, 1740–1748.
- [15] H. B. Aiyappa, J. Thote, D. B. Shinde, R. Banerjee, S. Kurungot, *Chem. Mater.* **2016**, *28*, 4375–4379.
- [16] B. Wurster, D. Grumelli, D. Hotger, R. Gutzler, K. Kern, *J. Am. Chem. Soc.* **2016**, *138*, 3623–3626.
- [17] L. K. Blusch, O. Mitevski, V. Martin-Diaconescu, K. Pröpper, S. DeBeer, S. Dechert, F. Meyer, *Inorg. Chem.* **2014**, *53*, 7876–7885.
- [18] A. Fuerte, A. Corma, M. Iglesias, E. Morales, F. Sánchez, *Catal. Lett.* **2005**, *101*, 99–103.
- [19] P. Manna, J. Debgupta, S. Bose, S. K. Das, *Angew. Chem. Int. Ed.* **2016**, *55*, 2425–2430; *Angew. Chem.* **2016**, *128*, 2471–2476.
- [20] J. J. Stracke, R. G. Finke, *J. Am. Chem. Soc.* **2011**, *133*, 14872–14875.
- [21] a) A. Mahammed, B. Mondal, A. Rana, A. Dey, Z. Gross, *Chem. Commun.* **2014**, *50*, 2725–2727; b) H. Lei, H. Fang, Y. Han, W. Lai, X. Fu, R. Cao, *ACS Catal.* **2015**, *5*, 5145–5153; c) S. Maji, I. López, F. Bozoglian, J. B.-Buchholz, A. Llobet, *Inorg. Chem.* **2013**, *52*, 3591–3593.
- [22] Y. Z. Han, Y. Z. Wu, W. Z. Lai, R. Cao, *Inorg. Chem.* **2015**, *54*, 5604–5613.
- [23] P. M. Usov, S. R. Ahrenholtz, W. A. Maza, B. Stratakes, C. C. Epley, M. C. Kessinger, J. Zhu, A. J. Morris, *J. Mater. Chem. A* **2016**, *4*, 16818–16823.
- [24] A. D. Becke, *J. Chem. Phys.* **1993**, *98*, 5648–5652.
- [25] G. A. Petersson, M. A. Al-Laham, *J. Chem. Phys.* **1991**, *94*, 6081–6090.

- [26] N. V. Krishna, J. V. S. Krishna, S. P. Singh, L. Giribabu, L. Han, I. Bedja, R. K. Gupta, A. Islam, *J. Phys. Chem. C* **2017**, *121*, 6464–6477.
- [27] Y. Lin, L. C. Chuang, Y. C. Lin, C. L. Lin, *Dalton Trans.* **2004**, *0*, 4006–4009.
- [28] Rita Giovannetti, *The Use of Spectrophotometry UV/Vis for the Study of Porphyrins, Macro To Nano Spectroscopy* (Ed.: Jamal Uddin), InTech, <https://doi.org/10.5772/38797>, **2012**, available from <https://www.intechopen.com/books/macro-to-nano-spectroscopy/the-use-of-spectrophotometry-uv-vis-for-the-study-of-porphyrins>.
- [29] J. Bard, L. R. Faulkner, *Electrochemical Methods Fundamentals and Applications*, 2nd ed., Wiley, New York, **2006**.

---

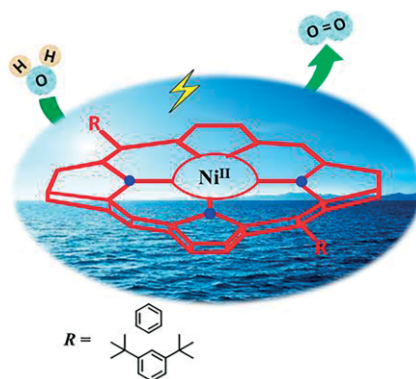
Received: December 8, 2017

## Water Splitting

J. V. S. Krishna, N. V. Krishna,  
S. K. Singh, P. K. Shaw,  
V. M. Dhavale,\* A. K. Vardhaman,\*  
L. Giribabu\* ..... 1–8



**Substituent-Induced Deformed Ni-Porphyrin as an Electrocatalyst for the Electrochemical Conversion of Water into Dioxygen**



The activities of 5,15-diphenylporphinatonicel(II) (**A**) and 5,15-bis(3,5-di-*tert*-butylphenyl)porphinatonicel(II) (**B**) complexes in the oxygen evolution reaction (OER) have been investigated in an alkaline medium. The OER activities of **A** and **B** have been correlated with their molecular properties.

DOI: 10.1002/ejic.201701427